High Quality Mn-Doped (Na,K)NbO$_3$ Nanofibers for Flexible Piezoelectric Nanogenerators

Han Byul Kang,[†] Jiyoung Chang,[‡] Kisik Koh,[‡] Liwei Lin,[‡] and Yong Soo Cho*,[†]

[†]Department of Materials Science and Engineering, Yonsei University, Seoul 120-749, Korea

[‡]Berkeley Sensor and Actuator Center, Department of Mechanical Engineering, University of California at Berkeley, Berkeley, California 94720, United States

ABSTRACT: Enhanced piezoelectric and energy-harvesting characteristics of Mn-doped $(Na_{0.5}K_{0.5})NbO_3$ (NKN) nanofibers have been investigated with actual fabrication of potential flexible nanogenerators. The electrospinning process of nanofibers has been initially optimized with the proper level of chelating agent and annealing temperature. High quality nanofibers are successfully obtained only by means of a certain level of doped-Mn, which incorporates into the NKN perovskite structure and facilitates significant grain growth. A single-particle-stacked structure along the direction of fiber length becomes more evident with increasing Mn content. An XPS analysis confirms that Mn exists in multivalent states of Mn^{2+}/Mn^{3+}. The effective piezoelectric coefficient of the nanofibers is found to be enhanced by 5 times with Mn-doping up to 3 mol % as characterized by piezoelectric force microscopy. The resultant flexible nanogenerators on PES films have exhibited ~0.3 V output voltage and ~50 nA output current under a bending strain.

KEYWORDS: (Na,K)NbO$_3$, piezoelectric properties, nanofiber, nanogenerator
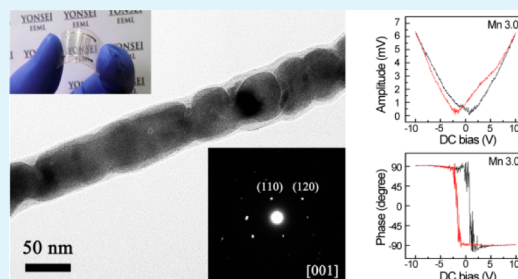
INTRODUCTION

Piezoelectric energy harvesting has been attractive as a promising power source for small self-powered electronic devices and wireless sensors. Because the power consumption of nano/micro devices is typically in the range of micro- to milliwatts, this harvesting technique is presumably applicable to generating power for specified devices.[1,2] Moreover, it can be operated regardless of the restriction in time and place because energy sources for mechanical vibration are easily available from surrounding environments. For high performance piezoelectric energy harvesters, it is essential to design efficiently harvesting structures combined with suitable piezoelectric materials and processing.

Electrospinning has been extensively studied as a promising technique for preparing controlled nanofibers since the processing procedure is relatively simple and cost-effective.[3] In recent years, numerous attempts have been made to obtain high quality piezoelectric nanofibers by the electrospinning process. For examples, Wang et al.[4] reported that nanoscale lead zirconate titanate (PZT) fibers could be achieved by electrospinning. Chang et al.[5] successfully fabricated poly(vinylidene fluoride) (PVDF) nanofibers patterned directly by using near-field electrospinning. There have been several reports on piezoelectric nanogenerators based on PZT nanofibers prepared by electrospinning.[6,7]

On the other hand, studies on Pb-free piezoelectric nanofibers have been very limited probably due to the difficulty in achieving high quality nanostructures. There are very limited reports on nanostructured (Na,K)NbO$_3$ (NKN) materials even though the piezoelectric characteristics of modified NKN bulk materials are very competitive compared to those of PZT materials.[8−10] Jalian and Girishin[11] introduced biocompatible (Na,K)NbO$_3$ nanofibers with an average diameter of 150 nm by electrospinning. They characterized the (Na,K)NbO$_3$ nanofibers as in a superparaelectric state with spontaneous electric polarization but without providing piezoelectric properties of nanofibers. There has been so far no report on piezoelectric properties and energy harvesting characteristics, which are specified for the Pb-free (Na,K)NbO$_3$ nanofibers.

In this work, we first report the piezoelectric properties of (Na,K)NbO$_3$ nanofibers optimized with the level of a chelating agent at various annealing temperatures. On the basis of several of our doping studies, Mn-doping was selected for higher quality nanofibers that are distinguished as continuous structure with higher crystallinity. The improved crystallinity must be responsible for enhancement in resultant flexible nanogenerators. The Mn-doping produces the 5× enhancement in piezoelectric coefficient d$_{33}$, compared to the undoped sample. This work concerns the fabrication of competitive nanogenerators using easily processable high quality nanofibers doped with Mn. A flexible piezoelectric nanogenerator is able to generate an output voltage of ~0.3 V and a current of ~50 nA by simple bending operation, even though the outcomes may be not meaningful without further optimization.

■ EXPERIMENTAL SECTION

Mn-doped $(Na_{0.5}K_{0.5})NbO_3$ (NKN) nanofibers were produced by an electrospinning process using common solutions. Potassium acetate (CH_3COOK, Sigma-Aldrich Inc., USA), sodium acetate (CH_3COONa, Daejung Co., Korea), and niobium ethoxide (Nb-$(OCH_2CH_3)_5$, Sigma-Aldrich Inc., USA) were dissolved into 2-methoxyethanol ($CH_3OCH_2CH_2OH$; Sigma-Aldrich Inc., USA) in a glovebox. Acetic acid (AAc, CH_3CO_2H, Ducksan Chemicals, Korea) was added into the solution as a chelating agent to have quality fibers as reported elsewhere.[12−14] The molar ratio of AAc/NKN solution was chosen as 0.0, 0.25, 0.5, 1.0, and 2.5.

Manganese acetate tetrahydrate ($(CH_3COO)_2Mn\cdot4H_2O$, Sigma-Aldrich Inc., USA) was dissolved into the AAc/NKN solution with different Mn contents of 0.0, 0.5, 1.0, and 3.0 mol %. In addition, polyvinylpyrolidone (PVP) ($(C_6H_9NO)_n$, M_w = 1 300 000 g/mol, Sigma-Aldrich Inc., USA) was incorporated into the Mn-doped AAc/NKN solution to obtain an appropriate viscosity of solution for effective spinning process. For complete dissolution, the resultant solution was stirred for 6 h at room temperature.

The final Mn-doped NKN solution was electrospun under 13 kV of electric field with a spray rate of 10 μL/min. The distance between needle tip and metal collector was about 10 cm. The electrospinning process was conducted on Si substrates in a closed box maintained at a relative humidity level of less than 30%. For better alignment of nanofibers, two pieces of conductive collectors were positioned in parallel sides of the Si substrate.[15] Nanofibers were annealed at 750 °C for an hour with 2 °C/min of heating rate in air.

Crystal structure of NKN nanofibers was investigated by an X-ray diffractometer (XRD: Ultima IV, Rigaku). Grain size, surface microstructure, and morphology of nanofibers were analyzed by field-emission scanning electron microscopy (FE-SEM: JSM 7001F, JEOL) and high resolution transmission electron microscopy (HRTEM: JEM-2100F, JEOL). The valence state of selected elements was studied by X-ray photoelectron spectroscopy (XPS: K-alpha, Thermo VG) using a monochromated Al X-ray source (Al Kα line: 1486.6 eV).

Ferroelectric hysteresis loops and piezoelectric properties of the nanofibers were measured by piezoelectric force microscopy (PFM: Nanoscope V Multimode, Bruker). The PFM samples were prepared on Pt/Ti/Si substrates acting as a bottom electrode holder. The mechanical oscillations of piezoelectric samples were induced by applying an ac field between the tip and holder. A Pt/Ir-coated silicon cantilever was used for this experiment under the condition of a spring constant of ~42 N/m and a resonance frequency of 330 kHz. Driving amplitude and frequency of ac bias were 5 V rms and 5 kHz, respectively. Each quantitative measurement by PFM was calibrated by using a standard piezoelectric response sample of commercially available periodically poled lithium niobate (PPLN) crystal. The amplitude of PR oscillations was translated from volts to picometers by setting up a deflection sensitivity of the cantilever from the measurement of the standard sample. Local piezoelectric hysteresis loop was measured by applying a dc bias ranging from −10 V up to 10 V.

To fabricate flexible nanogenerators, annealed NKN nanofibers were transferred to a flexible polyether sulfone (PES) substrate using polydimethylsiloxane (PDMS) (Sylgard 184, Dow Corning Corp., USA). The substrate size was 25 mm × 15 mm with ~200 μm in thickness. PDMS was spin-coated at 3000 rpm for 3 min on the PES substrate. To improve the contact between nanofibers and Pt electrodes, dry etching of PDMS was conducted at 150 W at 150 mTorr for 5 min by using reactive ion etching (RIE). A Pt electrode with ~100 nm in thickness was deposited in an interdigitated pattern on PDMS by DC sputtering. The distance between adjacent electrodes was 500 μm. The transference of nanofibers and their connection to electrodes were confirmed by optical microscopy. In order to enhance the mechanical stability of nanofibers, the fabricated structure was passivated by spin-coating of PDMS under the same coating condition as described above and also in a similar process used previously.[16] The nanogenerators were polled by applying an electric field of 60 kV/cm across the interdigitated electrodes at 100 °C for 30 min. Output voltage was recorded by a nanovoltmeter (2182A, Keithley) in a bending tester when a regular bending strain was applied onto the sample. A galvanostat (IviumStat, Ivium technologies) system was used to detect output current. Under the same condition, a switching polarity test was performed by interchanging the connection between the sample and the measuring machine.

■ RESULTS AND DISCUSSION

Prior to the investigation on the effects of Mn doping, physical quality of NKN nanofibers was initially optimized with regard to the relative content of AAc and annealing temperature. It seems that the existence of AAc helps in obtaining more homogeneous nanofibers by chelating solutions with a capability of viscosity controller.[12−14,17] The average diameter of electrospun nanofibers was maintained at nearly ~300 nm even when the molar ratios of AAc/NKN solution was increased to above 0.5. The diameter was dramatically reduced to ~130 nm after annealing at 750 °C. According to XRD analysis (not shown here), the 750 °C annealed sample showed phase-pure NKN crystalline phase. The as-prepared nanofibers were initially amorphous (up to 400 °C) and then became crystallized at 450 °C. Interestingly, the annealing at temperature higher than 850 °C was found to induce the secondary phase of $K_4Nb_6O_{17}$ possibly from the evaporation of the alkali ions. Accordingly, the molar ratio of 0.5 of AAc/NKN and the annealing temperature of 750 °C were used for further investigation on the effect of Mn-doping.

Figure 1 shows the XRD patterns of nanofibers containing different contents of Mn. Regardless of Mn content, phase-pure
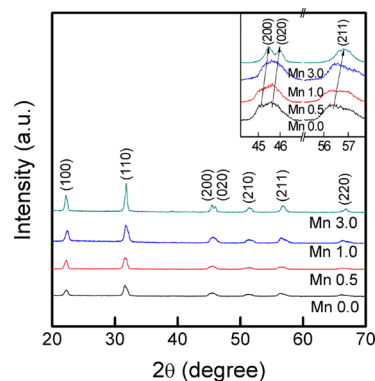

Figure 1. XRD patterns for Mn-doped NKN nanofibers annealed at 750 °C. The inset patterns at certain 2θ angles of 44−47° and 65−68° represent the shift in peak positions with Mn-doping.

NKN perovskite structure [JCPDS No. 77−0038] was identified without secondary phase. Increasing the Mn content tends to enhance the crystallinity of the perovskite phase by showing higher intensity peaks with more distinct peak splitting as exemplified with the (200) and (020) peaks. Crystalline size was calculated by using the known Sherrer equation from the full width at half-maximum (fwhm) of the (110) peak. The crystallite size of the films was found to increase gradually from ~12.3 nm to ~21.9 nm as the Mn content increased from 0 to 3 mol %, respectively.

It is believed that Mn is incorporated into the perovskite structure upon annealing, from the evidence that no Mn-involved secondary phase precipitates out. There is a report that Mn can be substituted for the A or B site in the structure up to 3 mol % in the bulk case.[18] The lattice distortion
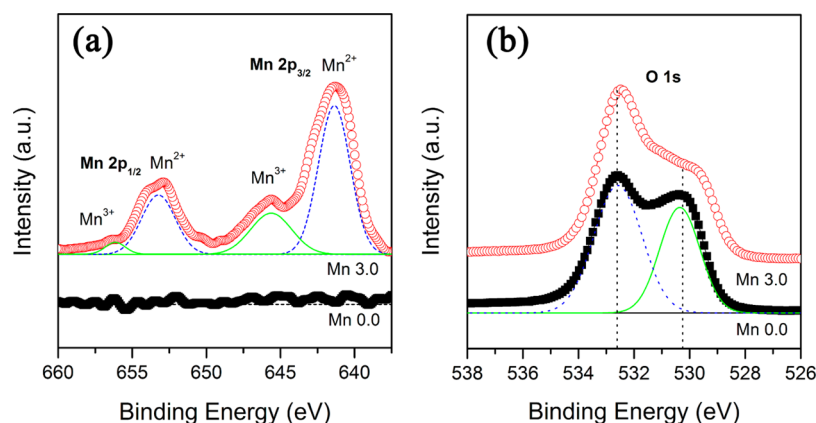
Figure 2. XPS profiles of undoped and 3 mol % Mn-doped NKN nanofibers for the valence state of (a) manganese in the 623−660 eV range and (b) oxygen in the 526−538 eV range. The peaks of the individual states were fitted with the Gaussian distribution curve for clear demonstration of peak splitting.

observed in the inset of Figure 1, where the (200) and (020) peaks at 45−46° tend to shift clearly toward higher angles, supports that Mn can be easily accommodated into the structure. When the ionic size of Mn^{2+} (0.72 Å) is considered in the precursor solution, the B site in the ABO_3 perovskite is likely to be mainly occupied. The ionic radius of Nb^{5+} (0.64 Å) is close enough for the Mn^{2+} size (compared to A site-ions, Na^{1+} (1.02 Å) and K^{1+} (1.38 Å)). As a result, the overall lattice parameters were found to decrease gradually with increasing content of Mn, which is further reasonable with the fact that the charge imbalance induced by the substitution of Nb^{5+} with Mn^{2+} may incur oxygen vacancies for charge compensation.[19,20]

Figure 2a shows the high-resolution XPS spectra of Mn 2p states in undoped and Mn-doped NKN nanofibers annealed at 750 °C. As expected, the Mn peaks were observed in the 640−660 eV range only in the case of Mn-doped sample. The peaks of Mn 2p states were fitted with the Gaussian distribution curve, resulting in two distinct components that are assigned as Mn^{3+} and Mn^{2+} in both $2p_{1/2}$ and $2p_{3/2}$ states. In the Mn $2p_{3/2}$ state, for example, the existence of both Mn^{2+} and Mn^{3+} were evident at ~641.3 eV (dashed line) and ~645.6 eV (solid line), respectively.[21] From the significant evolution of Mn^{2+} peak, it is confirmed that Mn^{2+} is dominantly present over Mn^{3+} in the annealed films.

Asymmetric and broad peaks, which were plotted by two different kinds of O species, were observed in the O 1s spectrum as shown in Figure 2b. The O 1s profile at around ~530.1 eV is identified as lattice oxygen (O_L) in the perovskite; the other peak at around ~532.5 eV is assigned as absorbed oxygen (O_a) that is related to hydroxyl group.[22−24] For Mn-doped NKN nanofibers, slight peak shifts toward the lower binding energy were observed due presumably to lattice distortion. The relative ratio of O_a/O_L is significantly increased by the Mn-doping as evidenced in Figure 3b. It has been shown that the increase of O_a/O_L derives from the increased surface oxygen vacancies resulting from Mn-doping.[23] Hence, the variation of O_a/O_L in the O 1s spectrum is likely to be the evidence for the B-site substitution of Mn ions.

Figure 3 shows the SEM images of the NKN nanofibers processed with different levels of Mn-doping and then annealed at 750 °C. The dimensional stability seems to be kept regardless of Mn-doping levels even though considerable shrinkage happens during annealing. It is noticeable that ~300 nm in diameter of the as-deposited nanofiber became
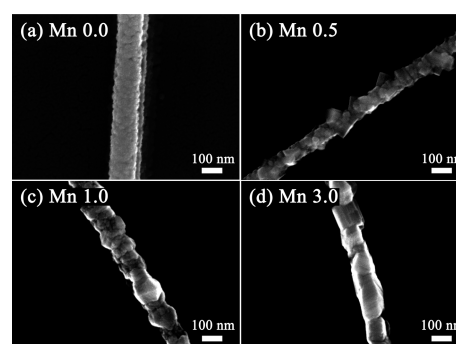

Figure 3. SEM images of Mn-doped NKN nanofibers annealed at 750 °C, containing (a) 0.0, (b) 0.5, (c) 1.0, and (d) 3.0 mol % Mn. Significant changes in morphology are evident with more Mn-doping.

~90 nm after annealing at 750 °C with 3 mol % Mn through the solvent evaporation and densification process.

As expected from the progress of crystallite evolution with Mn-doping in the XRD pattern of Figure 1, the changes in morphology with increasing Mn-doping are evident by showing more distinct grains along the direction of the length of nanofibers. Smaller grains found in undoped nanofibers were significantly enlarged by increasing the Mn content. Very large grains with a peculiar shape, which looks like a single particle stacked in the direction of the length of the fiber, are easily discernible in the case of 3.0 mol % Mn-doping (Figure 3d). It is clear that a small amount of the doped Mn encourages grain growth similarly as reported in the literature for the bulk perovskite materials including NKN, $BaTiO_3$, and Pb(Zr,Ti)-O_3.[19,25−27] The promotion of growth is associated with the creation of oxygen vacancies by the B-site (Nb^{5+}) substitution of Mn ions and thus the enhanced mobility of grain boundary to facilitate faster grain growth.[28,29]

The observation of the nanofibers via high-resolution TEM confirms the changed morphology driven by Mn-doping as shown in Figure 4. Again, a notable transition of morphology, i.e., the single-particle-chain shape, was clearly observed in the case of 3.0 mol % Mn-doping. This type of nanofiber was also reported in barium hexaferrites annealed at an elevated temperature with promising enhancement in magnetic properties.[30] Without Mn-doping, small crystallites are evidently observed with the supporting selected area electron diffraction (SAED) image standing for small overlapped crystallites
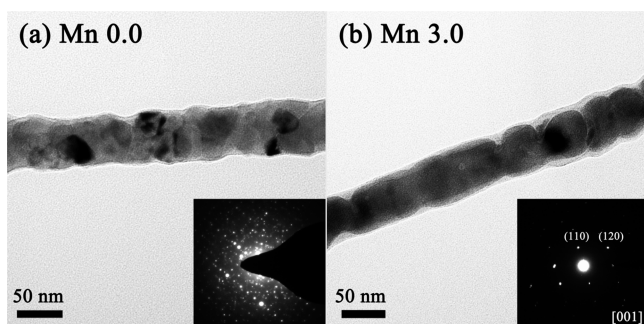
Figure 4. HR-TEM images of (a) undoped and (b) Mn-doped NKN nanofibers. The SAED pattern of each nanofiber is shown as an inset in each fiber.

although the direct comparison between nanofibers and thin films may not be very meaningful. Coercive voltage V_c, which is defined by the relation of $V_c = (V_c^+ - V_c^-)/2$ where V_c^+ and V_c^- are the starting points for switching polarization in the positive and negative bias, respectively, was slightly elevated with increasing of Mn concentration. Table 1 represents the H_c

Table 1. Normalized Coercive Field and Piezoelectric Coefficient $d_{33,eff}$ of Mn-Doped NKN Nanofibers, Which Were Obtained by Piezoelectric Force Microscopy

Mn (mol %)	0.0	0.5	1.0	3.0
Normalized $V_c{}^a$	1	1.03	1.44	1.79
$d_{33,eff}$ (pm/V)	7.27	9.35	22.25	40.06

^{a}Normalized to the value of 0 mol % Mn-doping sample.

(Figure 4a). In contrast, the SAED for 3 mol % Mn-doped sample corresponds to a diffraction pattern representing considerably grown perovskite crystallites. It is proposed that the Mn-doping is much more effective in creating well-defined grain structures than by means of raised annealing temperature (inducing also the alkali evaporation). This could be the main reason previous reports were not able to produce high quality NKN nanofibers via regular electrospinning and annealing processes.

Piezoelectric characteristics of Mn-doped NKN nanofibers were investigated by PFM. Figure 5 demonstrates the set of local piezoelectric responses (PR) of NKN nanofibers for samples with Mn-doping. The variation in PR amplitude (the upper graphs in Figure 5) as represented in a typical "butterfly loop" shape corresponds to the strain−electric field (S−E) curve of piezoelectric materials. In addition, the hysteresis loops with DC bias are illustrated with the PR phase (the bottom graphs in Figure 5). Those results indicate that the Mn-doped NKN nanofibers possess more distinct piezooelectricity. The difference of PR phase ($\Delta\Phi$) with the opposite signal is about 180°, which means the occurrence of 180° domain switching by the applied dc-bias. The applied voltage of 10 V corresponds to the electric field of ~80−110 kV/mm when the thickness of the NKN nanofibers is considered as 90−130 nm depending on the level of Mn-doping. The range of electric field is very similar to the reported range of 70−90 kV/mm for NKN thin films,

values normalized to that of the 0 mol % Mn sample to demonstrate the increasing effect with the addition of Mn. It is associated with the fact that Mn^{2+} substitutes the B-site and corresponds to the hard doping effect that brings the increase in coercive field similar to the studies of piezoelectric thin films.[26,31,32] It means that a higher field is required for the domain reversal with the Mn-doping. As reported in the case of Mn-doped NKN films,[33] the Mn-doping may induce significant domain wall pinning.

Meanwhile, the PR amplitude was significantly enhanced with more Mn-doping. These piezoresponses can be converted to the effective piezoelectric coefficient $d_{33,eff}$ and their average values are listed in Table 1. The piezoelectric coefficient was calculated by using a known relation of $\Delta u = \delta \times A = d_{33,eff} \times V_{ac}$, where Δu is the piezoresponse displacement, A is the obtained PR amplitude, δ is the deflection sensitivity of the cantilever, and V_{ac} is the amplitude of the driving ac voltage.[34] The improvement of the piezoelectric coefficient is observed with the addition of Mn. The coefficient is reached to 40.07 pm/V at 3.0 mol % of Mn, which is 5 times larger than the value for the sample without Mn. This significant improvement here can be attributed to the enhanced crystallinity and significant progress of densification with the Mn-doping. As another possible contributor, the increase in grain size reduces
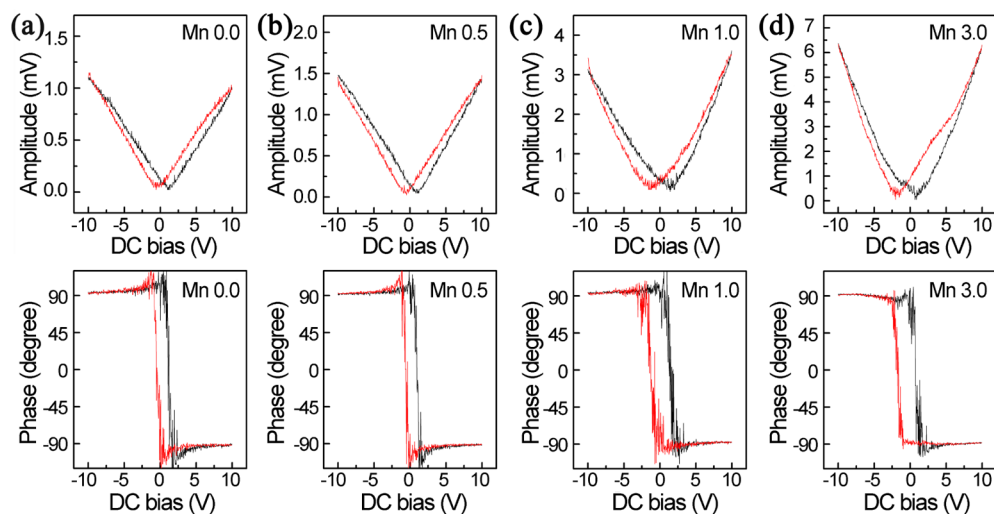

Figure 5. Variations of piezoelectric properties of $(Na,K)NbO_3$ nanofibers with Mn-doping, as represented by piezoresponse amplitude (top figures) and phase (bottom figures) diagrams for (a) 0.0, (b) 0.5, (c) 1.0, and (d) 3.0 mol % Mn-doped samples.
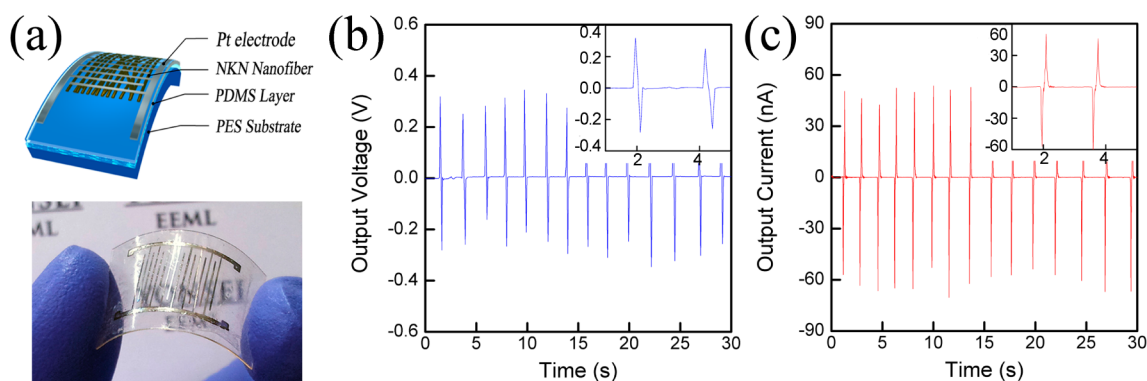
Figure 6. (a) Schematic of flexible piezoelectric nanogenerator based on a Mn-NKN/PDMS structure on PES film (with a real image of the nanogenerator), (b) output voltage, and (c) output current of the piezoelectric nanogenerator as a function of time, with the magnified peaks in the insets.
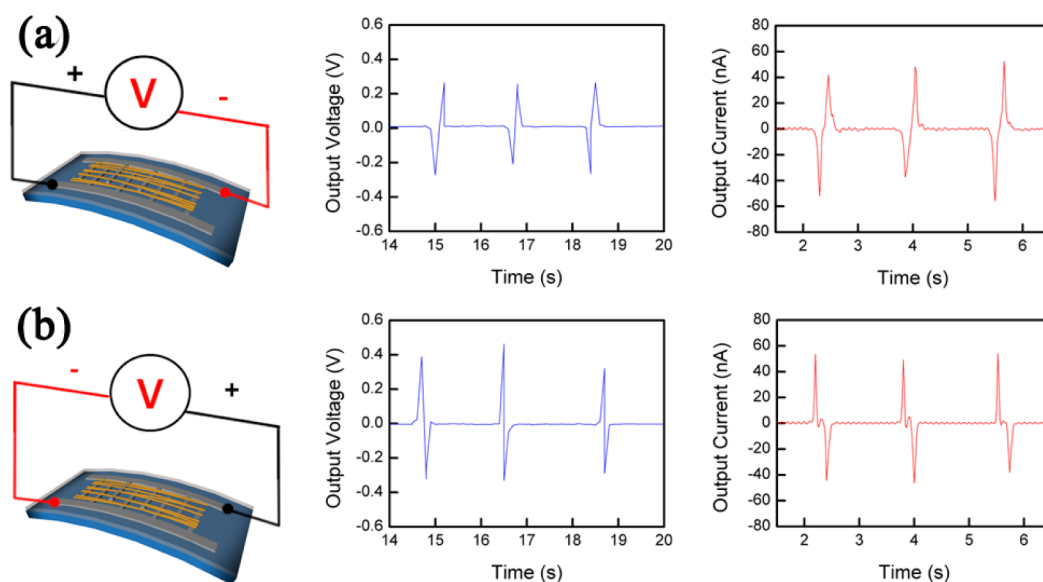

Figure 7. Switching polarity evaluation of output voltage and current in the piezoelectric nanogenerator for (a) forward connection and (b) backward connection, with schematic illustrations, indicating that the signals are based on piezoelectric response.

the density of the grain boundary so that the movement of the domain wall is less restricted by grain boundaries.[35,36]

Flexible piezoelectric nanogenerators based on Mn-doped NKN nanofibers were fabricated as illustrated in the schematic of Figure 6a. Output performance of the nanogenerators is represented in Figure 6b,c. When a bending strain is applied to the flexible nanogenerator, the NKN/PDMS film is subjected to tensile strain. As a result, the resulting piezoelectric potential difference is initiated between two electrode ends of piezoelectric nanofibers by a converse piezoelectric effect.[37] The piezoelectric potential difference leads to a free electron flow occurring from two parallel electrodes. Then, the electrons move around the external circuit and are detected as an output signal. The representative open-circuit voltage and current values are ~0.3 V and ~50 nA for the 3 mol % Mn-doped nanofibers, respectively. These values do not look great compared to the recent performance of other nanogenerators, but the optimization of the nanofiber-driven nanogenerators is not specified in this work. Enhancement in piezoelectricity of the applicable Pb-free nanofibers may be more meaningful at this stage with great potential as a nanogenerator with better structural adjustment in the future.

Figure 7 shows the result of switching polarity test for the 3 mol % Mn-doped sample to verify that the output signal is based on the piezoelectric nature of aligned nanofibers. The schematics of applying opposite bias for alternative connections in the nanogenerators are also included. The opposite sequence of peak occurrence with time according to the ± direction of bias confirms that the output signals originate from the piezoelectricity of Mn-doped NKN nanofibers. In addition, the output voltage of a reference device without nanofibers was measured to evaluate the contribution of the capacitance effect from materials other than nanofibers. The signals are negligible as ~4×10^{-10} V compared to the nanogenerator's output voltage of ~0.3 V. Accordingly, it is concluded that the performance of nanogenerators comes from the piezoelectric effect of the NKN nanofibers themselves. The flexible nanogenerators have good mechanical stability even after repetitive folding−releasing evaluations and could be a promising candidate for portable energy harvesters targeting implantable and wearable electronics applications.

■ CONCLUSIONS

High quality $(Na_{0.5}K_{0.5})NbO_3$ nanofibers containing small contents of Mn were prepared by electrospinning. The existence of Mn helps crystallite growth, leading to the formation of single-particle-chain shaped nanofibers with the apparent enhancement of piezoelectric properties. It is believed that Mn atoms are incorporated into the B site of perovskite NKN structure with lattice distortion as mixed-valence states of Mn^{2+}/Mn^{3+} and surface oxygen vacancy as confirmed by the XPS analysis. Nanofibers with 3 mol % Mn-doping have exhibited an effective piezoelectric coefficient of ~40.06 pm/V, which is 5 times higher than that of NKN nanofibers without Mn. Flexible piezoelectric nanogenerators based on a Mn-NKN/PDMS structure are successfully demonstrated on PES films with good mechanical stability even though output voltage and current values need to be further optimized.

■ AUTHOR INFORMATION

Corresponding Author
*Tel: 82-2-2123-5848. E-mail: ycho@yonsei.ac.kr.

Notes
The authors declare no competing financial interest.

■ ACKNOWLEDGMENTS

■ REFERENCES

(1) Fang, X. Q.; Liu, J. X.; Gupta, V. Fundamental Formulations and Recent Achievements in Piezoelectric Nano-Structures: A Review. *Nanoscale* **2013**, *5*, 1716−1726.

(2) Joseph, A. P. Energy Scavenging for Mobile and Wireless Electronics. *IEEE Pervasive Computing* **2005**, *4*, 18−27.

(3) Greiner, A.; Wendorff, J. H. Electrospinning: A Fascinating Method for the Preparation of Ultrathin Fibers. *Angew. Chem., Int. Ed.* **2007**, *46*, 5670−5703.

(4) Wang, Y.; Furlan, R.; Ramos, I.; Santiago-Aviles, J. J. Synthesis and Characterization of Micro/Nanoscopic $Pb(Zr_{0.52}Ti_{0.48})O_3$ Fibers by Electrospinning. *Appl. Phys. A: Mater. Sci. Process.* **2004**, *78*, 1043−1047.

(5) Chang, C. E.; Tran, V. H.; Wang, J. B.; Fuh, Y. K.; Lin, L. W. Direct-Write Piezoelectric Polymeric Nanogenerator with High Energy Conversion Efficiency. *Nano Lett.* **2010**, *10*, 726−731.

(6) Wu, W.; Bai, S.; Yuan, M.; Qin, Y.; Wang, Z. L.; Jing, T. Lead Zirconate Titanate Nanowire Textile Nanogenerator for Wearable Energy-Harvesting and Self-Powered Devices. *ACS Nano* **2012**, *6*, 6231−6235.

(7) Gu, L.; Cui, N.; Cheng, L.; Xu, Q.; Bai, S.; Yuan, M.; Wu, W.; Liu, J.; Zhao, Y.; Ma, F.; Qin, Y.; Wang, Z. L. Flexible Fiber Nanogenerator with 209 V Output Voltage Directly Powers a Light-Emitting Diode. *Nano Lett.* **2012**, *13*, 91−94.

(8) Saito, Y.; Takao, H.; Tani, T.; Nonoyama, T.; Takatori, K.; Homma, T.; Nagaya, T.; Nakamura, M. Lead-Free Piezoceramics. *Nature* **2004**, *432*, 84−87.

(9) Ming, B. Q.; Wang, J. F.; Qi, P.; Zang, G. Z. Piezoelectric Properties of (Li, Sb, Ta) Modified $(Na,K)NbO_3$ Lead-Free Ceramics. *J. Appl. Phys.* **2007**, *101*, 054103.

(10) Zuo, R.; Fu, J.; Lv, D. Phase Transformation and Tunable Piezoelectric Properties of Lead-Free $(Na_{0.52}K_{0.48-x}Li_x)$-$(Nb_{1-x-y}Sb_yTa_x)O_3$ System. *J. Am. Ceram. Soc.* **2009**, *92*, 283−285.

(11) Jalalian, A.; Grishin, A. M. Biocompatible Ferroelectric $(Na,K)NbO_3$ Nanofibers. *Appl. Phys. Lett.* **2012**, *100*, 012904.

(12) Wu, A. Y.; Vilarinho, P. M.; Salvado, I. M. M.; Baptista, J. L. Sol-Gel Preparation of Lead Zirconate Titanate Powders and Ceramics: Effect of Alkoxide Stabilizers and Lead Precursors. *J. Am. Ceram. Soc.* **2000**, *83*, 1379−1385.

(13) Zhang, M.; Salvado, I. M. M.; Vilarinho, P. M. Synthesis and Characterization of Lead Zirconate Titanate Fibers Prepared by the Sol-Gel Method: The Role of the Acid. *J. Am. Ceram. Soc.* **2003**, *86*, 775−781.

(14) Malic, B.; Arcon, I.; Kodre, A.; Kosec, M. Homogeneity of $Pb(Zr,Ti)O_3$ Thin Films by Chemical Solution Deposition: Extended X-ray Absorption Fine Structure Spectroscopy Study of Zirconium Local Environment. *J. Appl. Phys.* **2006**, *100*, 051612.

(15) Li, D.; Wang, Y. L.; Xia, Y. N. Electrospinning Nanofibers as Uniaxially Aligned Arrays and Layer-by-Layer Stacked Films. *Adv. Mater.* **2004**, *16*, 361−366.

(16) Chang, J.; Lin, L. Large Array Electrospun PVDF Nanogenerators on a Flexible Substrate. In *Proceedings of Solid-State Sensors, Actuators and Microsystems Conference*, Transducers 2011, Beijing, China, June 5−9, 2011; pp 747−750.

(17) Han, S. O.; Youk, J. H.; Min, K. D.; Kang, Y. O.; Park, W. H. Electrospinning of Cellulose Acetate Nanofibers Using a Mixed Solvent of Acetic Acid/Water: Effects of Solvent Composition on the Fiber Diameter. *Mater. Lett.* **2008**, *62*, 759−762.

(18) Jiang, X. P.; Wang, X. J.; Wen, J. X.; Chen, C.; Tu, N.; Li, X. H. Microstructure and Electrical Properties of Mn-Modified Bismuth-Layer $Na_{0.25}K_{0.25}Bi_{2.5}Nb_2O_9$ Ceramics. *J. Alloy. Compd.* **2012**, *544*, 125−128.

(19) Zhu, M.; Liu, L.; Hou, Y.; Wang, H.; Yan, H. Microstructure and Electrical Properties of MnO-Doped $(Na_{0.5}Bi_{0.5})_{0.92}Ba_{0.08}TiO_3$ Lead-Free Piezoceramics. *J. Am. Ceram. Soc.* **2007**, *90*, 120−124.

(20) Chen, J.; Hu, Z.; Shi, H.; Li, M.; Dong, S. High-Power Piezoelectric Characteristics of Manganese-Modified $BiScO_3$-$PbTiO_3$ High-Temperature Piezoelectric Ceramics. *J. Phys. D: Appl. Phys.* **2012**, *45*, 465303.

(21) Hejazi, M. M.; Taghaddos, E.; Safari, A. Reduced Leakage Current and Enhanced Ferroelectric Properties in Mn-Doped $Bi_{0.5}Na_{0.5}TiO_3$-Based Thin Films. *J. Mater. Sci.* **2013**, *48*, 3511−3516.

(22) Lu, Y.; Lin, Y.; Xie, T.; Shi, S.; Fan, H.; Wang, D. Enhancement of Visible-Light-Driven Photoresponse of Mn/ZnO System: Photogenerated Charge Transfer Properties and Photocatalytic Activity. *Nanoscale* **2012**, *4*, 6393−6400.

(23) Jing, L.; Xin, B.; Yuan, F.; Xue, L.; Wang, B.; Fu, H. Effects of Surface Oxygen Vacancies on Photophysical and Photochemical Processes of Zn-Doped TiO_2 Nanoparticles and Their Relationships. *J. Phys. Chem. B* **2006**, *110*, 17860−17865.

(24) Wang, J.; Chen, W.; Wang, M. Properties Analysis of Mn-Doped ZnO Piezoelectric Films. *J. Alloy. Compd.* **2008**, *449*, 44−47.

(25) Lee, S. Y.; Ahn, C. W.; Ullah, A.; Seog, H. J.; Kim, J. S.; Bae, S. H.; Kim, I. W. Effect of Mn Substitution on Ferroelectric and Leakage Current Characteristics of Lead-Free $(K_{0.5}Na_{0.5})(Mn_xNb_{1-x})O_3$ Thin Films. *Curr. Appl. Phys.* **2011**, *11*, S266−S269.

(26) Mgbemere, H. E.; Hinterstein, M.; Schneider, G. A. Structural Phase Transitions and Electrical Properties of $(K_xNa_{1-x})NbO_3$-Based Ceramics Modified with Mn. *J. Eur. Ceram. Soc.* **2012**, *32*, 4341−4352.

(27) Jiang, M.; Lin, Q.; Lin, D.; Zheng, Q.; Fan, X.; Wu, X.; Sun, H.; Wan, Y.; Wu, L. Effects of MnO_2 and Sintering Temperature on Microstructure, Ferroelectric, and Piezoelectric Properties of $Ba_{0.85}Ca_{0.15}Ti_{0.90}Zr_{0.10}O_3$ Lead-Free Ceramics. *J. Mater. Sci.* **2013**, *48*, 1035−1041.

(28) Yu, C. S.; Hsieh, H. L. Piezoelectric Properties of Pb-$(Ni_{1/3}Sb_{2/3})O_3$-$PbTiO_3$-$PbZrO_3$ Ceramics Modified with MnO_2 Additive. *J. Eur. Ceram. Soc.* **2005**, *25*, 2425−2427.

(29) Lee, S. M.; Lee, S. H.; Yoon, C. B.; Kim, H. E.; Lee, K. W. Low-Temperature Sintering of MnO_2-Doped PZT-PZN Piezoelectric Ceramics. *J. Electroceram.* **2007**, *18*, 311−315.

(30) Zhang, J.; Fu, J.; Li, F.; Xie, E.; Xue, D.; Mellors, N. J.; Peng, Y. $BaFe_{12}O_{19}$ Single-Particle-Chain Nanofibers: Preparation, Characterization, Formation Principle, and Magnetization Reversal Mechanism. *ACS Nano* **2012**, *6*, 2273−2280.

(31) Zhu, W.; Fujii, I.; Ren, W.; Trolier-Mckinstry, S. Influence of Mn Doping on Domain Wall Motion in $Pb(Zr_{0.52}Ti_{0.48})O_3$ Films. *J. Appl. Phys.* **2011**, *109*, 064105.

(32) Luo, L.; Zhou, D.; Tang, Y.; Jia, Y.; Xu, H.; Luo, H. Effects of Mn Doping on Dielectric and Piezoelectric Properties of 0.71Pb-$(Mg_{1/3}Nb_{2/3})O_3$-0.29PbTiO₃ Single Crystals. *Appl. Phys. Lett.* **2007**, *90*, 102907.

(33) Wang, L.; Ren, W.; Shi, P.; Chen, X.; Wu, X.; Yao, X. Enhanced Ferroelectric Properties in Mn-doped $K_{0.5}Na_{0.5}NbO_3$ Thin Films Derived From Chemical Solution Deposition. *Appl. Phys. Lett.* **2010**, *97*, 072902.

(34) García, R.; Pérez, R. Dynamic Atomic Force Microscopy Methods. *Surf. Sci. Rep.* **2002**, *47*, 197−301.

(35) Cao, W.; Randall, C. A. Grain Size and Domain Size Relations in Bulk Ceramic Ferroelectric Materials. *J. Phys. Chem. Solids* **1996**, *57*, 1499−1505.

(36) Martirena, H. T.; Burfoot, J. C. Grain-Size Effects on Properties of Some Ferroelectric Ceramics. *J. Phys. C: Solid State Phys.* **1974**, *7*, 3182−3192.

(37) Wu, W.; Bai, S.; Yuan, M.; Qin, Y.; Wang, Z. L.; Jing, T. Lead Zirconate Titanate Nanowire Textile Nanogenerator for Wearable Energy-Harvesting and Self-Powered Devices. *ACS Nano* **2012**, *6*, 6231−6235.

10582

dx.doi.org/10.1021/am502234q | *ACS Appl. Mater. Interfaces* 2014, 6, 10576−10582